

Flávia Costa, Clarissa Canella,
Pedro Henrique Martins, and Silvana Mendonça

Contents

55.1	Introduction	1357
55.2	Fibroblastic/Myofibroblastic and Fibrohistiocytic Tumors	1358
55.3	Abscesses, Hematomas, and Necrotic Tumors	1358
55.4	Myxoid Tumors	1360
55.5	Small Round Blue Cell Tumors	1362
55.6	Monitoring Treatment	1363
	Conclusion	1366
	References	1366

Abbreviations

ADC	Apparent diffusion coefficient
Cho	Choline
CT	Computed tomography
DWI	Diffusion-weighted imaging
GCT	Giant cell tumor
MRI	Magnetic resonance imaging
MRS	Magnetic resonance spectroscopy
MSK	Musculoskeletal
ROI	Region of interest
SRBC	Small round blue cell
WHO	World Health Organization

55.1 Introduction

Magnetic resonance imaging (MRI) is the method of choice for the preoperative and post-treatment staging of musculoskeletal tumors [1]. The ability of MRI to identify and characterize the anatomic extent of musculoskeletal soft tissue tumors is well described [2]. In addition, MR imaging offers several advantages when compared with other methods in the evaluation and staging of soft tissue tumors considering high resolution, tissue contrast, and multiplanar capability [3].

Soft tissue sarcomas are rare neoplasms of mesenchymal origin. They constitute less than 1 % of all malignant tumors, with an incidence increasing slightly with age [2]. Unfortunately, for the majority, conventional MRI is incapable to provide

F. Costa, MD (✉) • C. Canella, MD
Clínica de Diagnóstico por Imagem,
Serviço de Radiologia e Diagnóstico por Imagem,
da Universidade Federal do Rio de Janeiro – UFRJ,
Rio de Janeiro, Brazil
e-mail: flavia26rio@hotmail.com

P.H. Martins, MD • S. Mendonça, MD
Clínica de Diagnóstico por Imagem,
Rio de Janeiro, Brazil

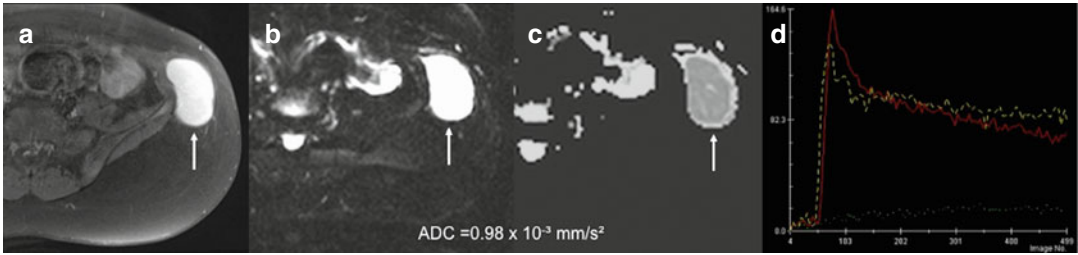


Fig. 55.1 Synovial sarcoma of the abdominal wall. (a) Axial T1 fat-suppressed MR image shows a hyperintense lesion in the soft tissue of the abdominal wall (arrow). Axial DWI (b) and ADC map (c) images show restricted diffusion (white arrows) of the lesion, with

$ADC=0.98 \times 10^{-3} \text{ mm}^2/\text{s}$, suggesting malignant tissue. (d) The tumor has a type IV curve with washout phase (yellow dotted line) on MR perfusion imaging, indicating that it enhances early at the same time as the artery. The red type IV curve indicates the artery

a precise histologic diagnosis (Fig. 55.1) and also to determine the extent of tumor necrosis that is essential to analyze response to treatment [1].

Besides several imaging modalities, radiographs are often the first-line investigation to differentiate bone tumors and to decide if MRI is necessary for diagnosis or staging [1]. MRI is also required when the lesion is indeterminate in radiographs and in local staging and when biopsy is necessary [1, 3].

Advanced MR imaging techniques, for example, diffusion-weighted imaging, dynamic contrast-enhanced imaging, proton MR spectroscopy (MRS), and inphase/opposed-phase imaging, can be used together with conventional images, to improve diagnostic accuracy and to evaluate the response to treatment [1, 3].

The aim of this chapter is to discuss the role of advanced MRI techniques in the workup of detection and characterization of soft tissue sarcomas and monitor response to treatment [3].

55.2 Fibroblastic/Myofibroblastic and Fibrohistiocytic Tumors

In adults, fibrous tumors are among the most common soft tissue lesions encountered in clinical practice [4]. These mesenchymal tumors are characterized histologically by the proliferation of fibroblasts and myofibroblasts, with marked production of intercellular collagen, and biologic behavior intermediate between that of benign lesions and malignant tumors [5].

MRI findings are typical and include bands of low signal intensity across all sequences and moderate to intense enhancement after contrast administration, although these findings are seen in benign and malignant fibrous tumors [3, 5]. In our experience, we have been observed that benign and intermediate fibrous tumors usually have facilitated diffusion, whereas malignant tumors have restricted diffusion on the ADC map (Fig. 55.2) [3].

Myositis ossificans is classified as a fibroblastic/myofibroblastic tumor, in accordance with the World Health Organization (WHO). This lesion is a benign, solitary, self-limiting, ossifying soft tissue mass usually occurring within skeletal muscle. A history of trauma is frequently elicited but is often absent [6]. Its MR appearance changes with the age of the lesion. During its early active phase, the lesion is immature and may show high perfusion as a result of neovascularity and may mimic a malignant neoplasm [6].

On DWI, myositis ossificans presents facilitated diffusion and a high ADC, suggesting benign tumor (Fig. 55.3) [3]. A follow-up examination after 2–4 weeks is suggested to confirm the diagnosis, avoiding unnecessary biopsy.

55.3 Abscesses, Hematomas, and Necrotic Tumors

Necrotic masses can be either malignant tumors or benign masses, such as abscesses and/or hematomas. Therefore, care must be taken during

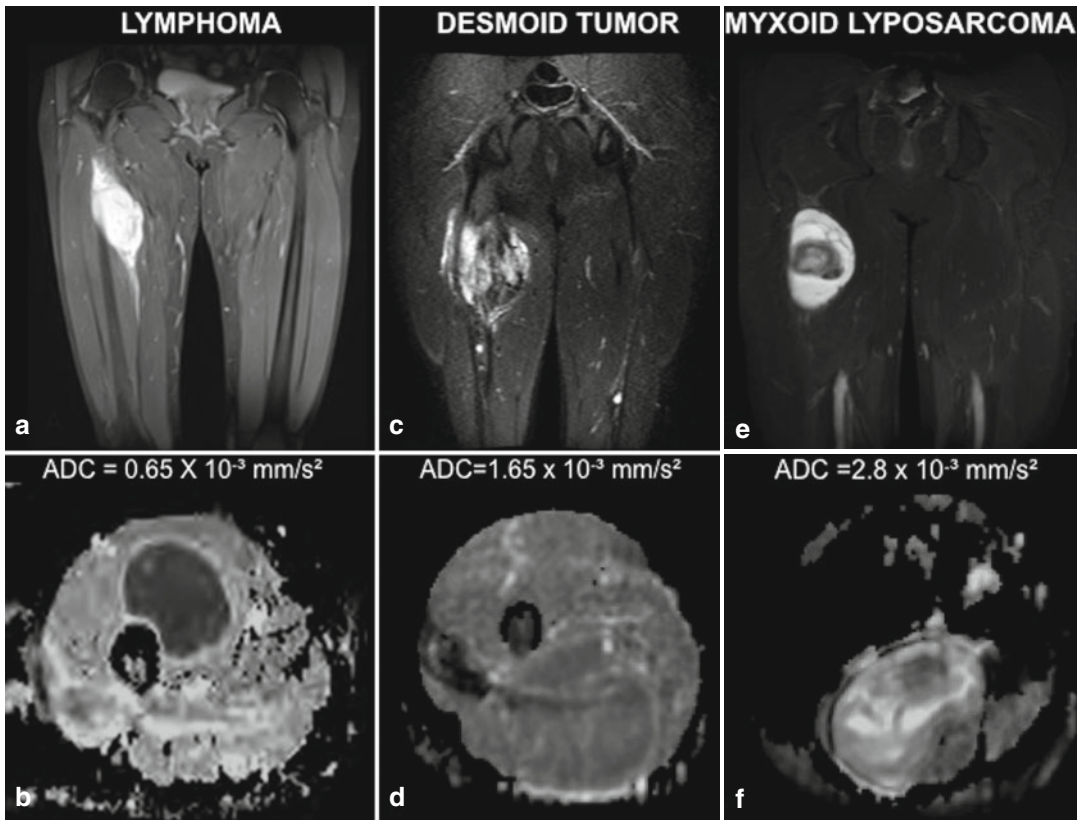


Fig. 55.2 Differentiation of lymphoma (a), desmoid tumor (c), and myxoid liposarcoma (e) of the left thigh, using DWI sequences. Note the homogeneous contrast enhancement of the lymphoma (a); the heterogeneous contrast enhancement of the desmoid tumor (c) within low signal intensity bands without contrast enhancement, suggesting collagen bands; and the heterogeneous lobular contrast enhancement of the myxoid liposar-

coma (e). Axial ADC map shows restricted diffusion of the lymphoma ($ADC=0.65 \times 10^{-3} \text{ mm/s}^2$) (b); facilitated diffusion ($ADC=1.65 \times 10^{-3} \text{ mm/s}^2$) of the desmoid tumor (d), indicating a benign lesion; and facilitated diffusion ($ADC=2.8 \times 10^{-3} \text{ mm/s}^2$) of the myxoid liposarcoma (f), despite the fact that the tumor is malignant, indicating the myxoid component of the lesion

imaging to differentiate a hemorrhagic malignant soft tissue tumor from a hematoma.

Abscesses contain inflammatory cells, a matrix of proteins, cellular debris, and bacteria in high-viscosity pus, with all of these factors restricting the motion of water. Hence, the abscess cavity is characterized by high signal intensity on DWI and decreased ADC value (Fig. 55.4) [7].

Necrotic malignant neoplasms tend to have more facilitated diffusion in their necrotic centers than do abscess cavities. Highly malignant tumors tend to have more restricted diffusion on the ADC map in the solid wall of the tumor, which has higher cellularity (Fig. 55.4) [3].

Like abscess, subacute hematomas present with restricted diffusion on the ADC map in the central portion of the lesion, but they have typical morphologic characteristics on conventional MR imaging. Therefore, the authors think that it is possible to differentiate abscesses and hematomas from malignant tumors using the ADC value from the necrotic portion of the tumor in conjunction with conventional MR imaging (Fig. 55.5).

Chronic expanding hematoma (CEH) is a gradually enlarging lesion that may be misdiagnosed as a hemorrhagic malignant soft tissue mass due to its size and progression. A recent report has shown that DWI could be used to

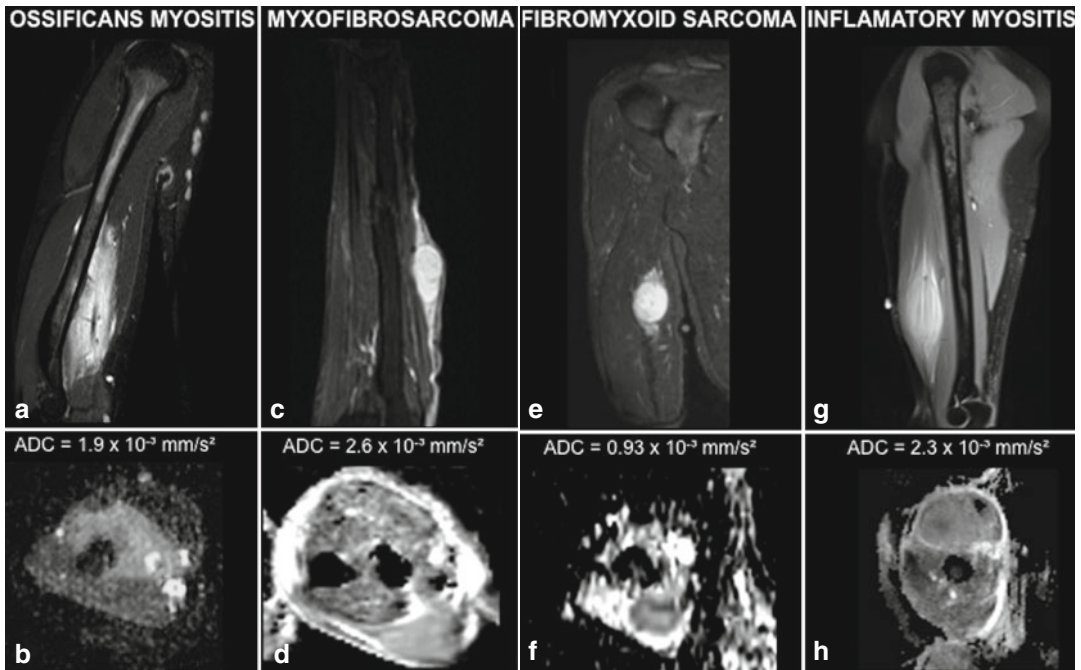


Fig. 55.3 Differentiation between ossificans myositis (**a**, **b**), myxofibrosarcoma (**c**, **d**), fibromyxoid sarcoma (**e**, **f**), and inflammatory myositis (**g**, **h**) with DWI sequences. Coronal T1-weighted fat-suppressed contrast-enhanced MR images of the ossificans myositis (**a**), myxofibrosarcoma (**c**), fibromyxoid sarcoma (**e**), and inflammatory myositis (**g**, **h**) show the homogeneous contrast enhancement of the lesions. Note that on inflammatory myositis, it is possible to identify muscle fibers underneath the lesion,

suggesting only infiltration of muscle fibers. ADC maps show facilitated diffusion of the ossificans myositis (**b**), myxofibrosarcoma (**d**), and inflammatory myositis (**h**), with ADC values of $1.9 \times 10^{-3} \text{ mm}^2/\text{s}^2$, $2.6 \times 10^{-3} \text{ mm}^2/\text{s}^2$, and $2.3 \times 10^{-3} \text{ mm}^2/\text{s}^2$, respectively. Fibromyxoid sarcoma (**f**) presented restricted diffusion on ADC maps ($\text{ADC} = 0.93 \times 10^{-3} \text{ mm}^2/\text{s}^2$), indicating a malignant tumor. Although from malignant origin, myxofibrosarcoma presents high ADC values because of the myxoid component

differentiate between these entities [8] because CEH can have similar appearances to hemorrhagic soft tissue sarcomas, but due to their low cellularity in solid wall, they have a significantly higher ADC value than a malignant mass on DWI.

Dynamic contrast-enhanced MR imaging demonstrates that abscesses may be highly vascularized and perfused lesions with slopes similar to those of malignant tumors (Fig. 55.4). In contrast, highly necrotic malignant tumors may have a low slope, similar to that of benign lesions [9]. Contrast enhancement in benign hematomas is rare [8].

After conventional MR imaging and determination of clinical history, advanced MR imaging techniques may be superior in differentiating abscesses and hematomas from malignant tumors.

55.4 Myxoid Tumors

Myxoid tissue is present in myxomas, myxoid liposarcomas, myxoid components of myxoid chondrosarcomas, and myxoid malignant fibrous histiocytomas [10].

The myxoid tumor matrix is characterized by high mucin and low collagen contents, representing a lesion composed of a large amount of water. Because of that, myxoid tumors have higher diffusion coefficients than nonmyxoid tumors, and this is true for both benign and malignant soft tissue myxoid tumors (Fig. 55.4) [3, 11–14]. ADC values of benign and malignant myxoid tumors may show substantial overlap [11], and DWI might be used in myxoid tumor diagnosis with caution.

Myxoid liposarcoma is a type of malignant fatty tumor, accounting for approximately

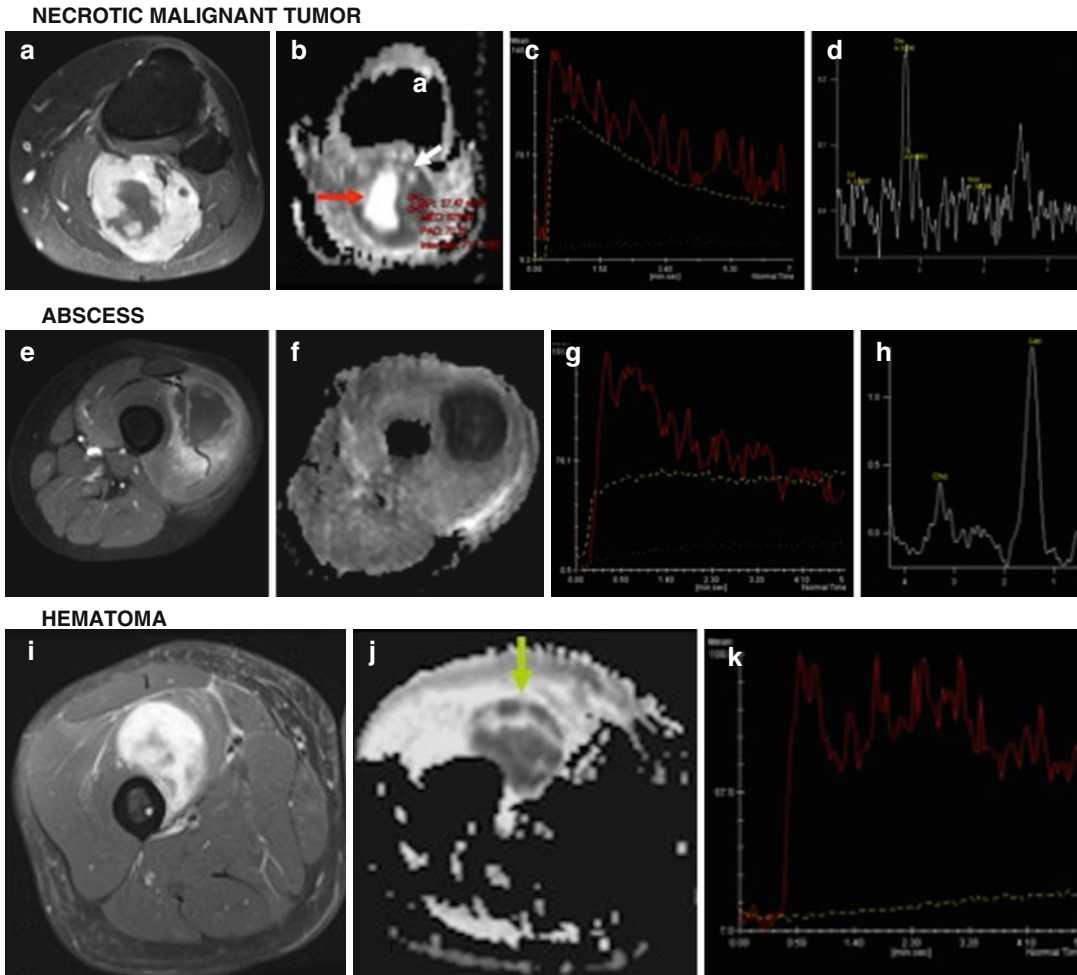


Fig. 55.4 Differentiation between necrotic malignant tumor (a, d), abscess (e–h), and hematoma (i–k) with DWI, MR perfusion imaging, and MR spectroscopy sequences. Axial T1-weighted fat-suppressed contrast-enhanced MR images of necrotic malignant tumor of the leg (a), an abscess in the thigh (e), and a hematoma in the thigh (i) show peripheral contrast enhancement of the lesions. ADC maps show restricted diffusion in the central portion in the abscess (f) and in the hematoma (j) (green arrow). The ADC map of the

necrotic tumor shows facilitated diffusion in the necrotic portion (b – red arrow) and restricted diffusion in the solid wall (b, white arrow), suggesting hypercellularity. MR perfusion imaging of the necrotic malignant tumor (c) shows a type IV “washout” curve (yellow dotted line), of the abscess (g) shows a type III curve (yellow dotted line), and of the hematoma (k) shows a type II curve (yellow dotted line). MR spectroscopy shows high levels of choline for the necrotic malignant tumor (d) and of lactate for the abscess (h)

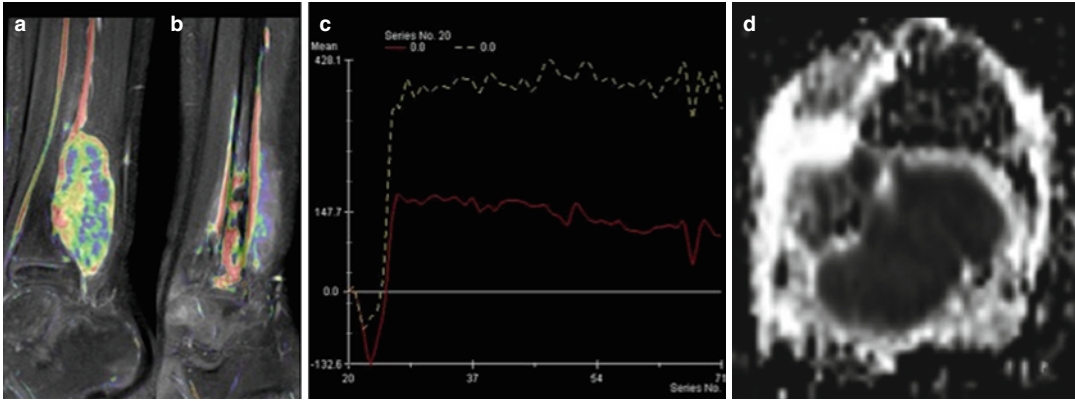
one-third of all liposarcomas. These tumors have low signal intensities on T1-weighted sequences and high signal intensities on T2-weighted sequences, occasionally resembling cysts [15], but have solid characteristics after contrast administration (Fig. 55.2).

Perfusion methods are useful for distinguishing cysts from myxoid tumors, because fluid does not enhance, whereas myxoid tissue in a sarcoma shows

intense and fast enhancement [10]. If a myxoid tumor shows rapid filling, then a myxoid-containing malignancy, such as a myxoid liposarcoma or synovial sarcoma, should be suspected [10].

An understanding of the morphologic MR imaging appearance as well as the perfusion and DWI characteristics of myxoid tumors may permit more accurate diagnosis in case of indeterminate soft tissue masses (Figs. 55.2 and 55.3) [3].

BEFORE TREATMENT



AFTER TREATMENT

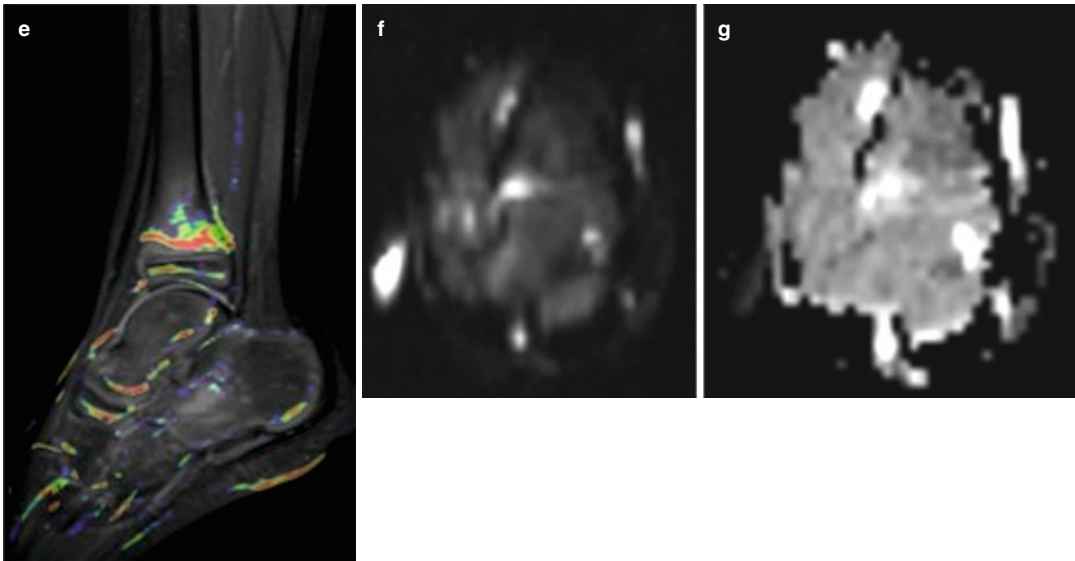


Fig. 55.5 Evaluation of response to treatment of an Ewing Sarcoma of the leg with dynamic contrast-enhanced MR imaging with color mapping. Before treatment: (a) Sagittal dynamic contrast-enhanced imaging with color mapping (b) shows many red regions in the tumor, suggesting hypervascularity. (c) The tumor has a type III curve (yellow dotted line) on MR perfusion imaging. The

red type IV curve indicates the artery. (d) The tumor presented restricted diffusion with $ADC=0.68 \times 10^{-3} \text{ mm}^2/\text{s}$, suggesting malignant tissue. After treatment: (e) sagittal dynamic contrast-enhanced imaging with color mapping shows important reduction in size of the tumor and of the red regions on color mapping and higher ADC value on DWI (f, g), indicating good response to treatment

55.5 Small Round Blue Cell Tumors

Small round blue cell (SRBC) tumors are a group of undifferentiated aggressive embryonal tumors, which have similar histologic features and immunohistochemistry, so alternative techniques are required to diagnose them.

Accurate diagnosis of these cancers is critical for the correct administration of therapy and for avoiding unnecessary patient procedures [3]. Currently, there is no widely available tool for real-time noninvasive diagnosis of soft tissue masses [3].

Ewing family tumors are more commonly skeletal; the extraskeletal form is much rarer, seen in the paravertebral regions, thoracic wall

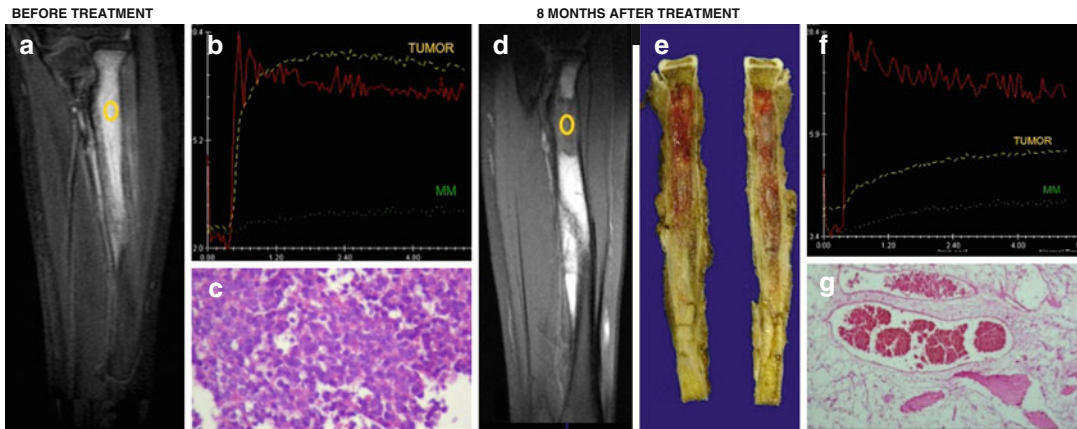


Fig. 55.6 Evaluation of response treatment of Ewing sarcoma of the radius by using dynamic contrast-enhanced imaging with color mapping. Pretreatment images (a–c) and posttreatment images (d–g) are shown. Pretreatment (a) coronal T1-weighted contrast-enhanced MR image shows the homogeneous enhancement of the lesion with a type III curve (yellow dotted line) on MR perfusion imaging (b). The green curve represents the muscle perfusion, and the red type IV curve indicates the artery. Slope=60 % for minute.

(c) The histopathological analyses show small round blue cell tumor. Posttreatment (8 months later) (d) coronal T1-weighted contrast-enhanced MR image shows lower enhancement of the tumor that now presents a type II curve (yellow dotted line) on MR perfusion imaging with a slope value=10 % for minute (f). Note that the tumor presented more than 40 % of reduction in slope value, indicating more than 90 % of response to therapy.(g) The histopathological analyses show necrosis after the treatment

(formerly known as Askin tumor), retroperitoneum, and lower extremities in older children or young adults (Figs. 55.5 and 55.6) [16].

Primary malignant involvement of soft tissues by extranodal lymphoma is rare, accounting for only 0.1–2 % of all soft tissue tumors [17]. More commonly, there is extension of a primary bone lymphoma into the surrounding tissues [18]. The primary soft tissue tumors are non-Hodgkin lymphomas, mostly of the B-cell type.

^1H MRS, which assesses the biochemical characteristics and metabolites of tumor tissue, may be a useful method of diagnosis of SRBC tumors because choline level increases in proportion to cellular proliferation and tumor malignancy [10, 19]. Choline peaks have been observed in malignant lymphomas [19, 20].

Malignant lymphomas have characteristically low ADC values in the brain [21], head and neck, and retroperitoneal regions [22]. Nagata and colleagues [12] have shown that soft tissue tumors have this property as well. Because of their high cellularity and nucleocytoplasmic ratio, lymphomas have a high signal intensity on DWI images. In addition, lymphomas have lower ADC values

than other tumor types in different body regions (Fig. 55.7) [22, 23].

In conclusion, in the differential diagnosis of a tumor with restricted diffusion on the ADC map and very low ADC value, SRBC tumors should be the main diagnostic hypothesis (Figs. 55.5 and 55.7). However, this conclusion must be corroborated by morphologic characteristics obtained using conventional MR imaging and other imaging methods.

55.6 Monitoring Treatment

MR imaging is essential for assessing the effectiveness of therapy, for planning further treatment, and for predicting patient prognosis [1, 24]. There are two settings in which MR imaging is used in the assessment of primary musculoskeletal tumors following treatment: after neoadjuvant therapy to define the extension of the lesion after treatment to help determine treatment response and after surgery to detect residual or recurrent tumor, distinguishing then from postoperative fibrosis or inflammation [25].

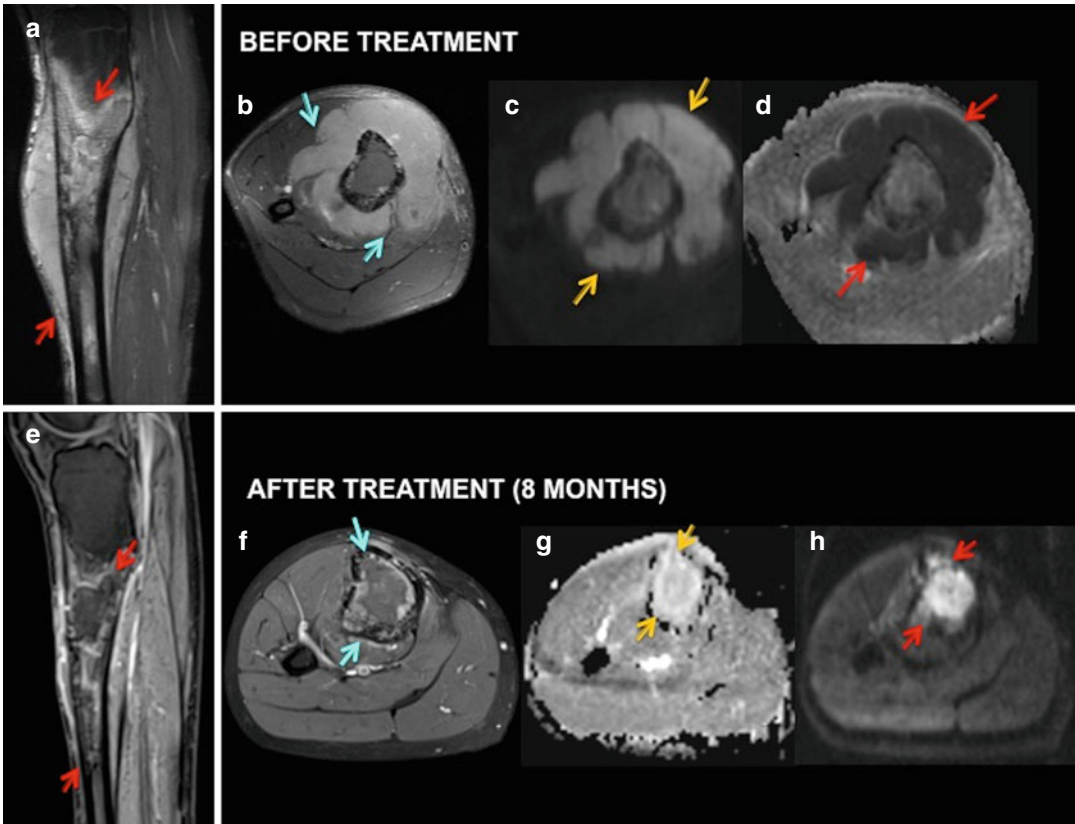


Fig. 55.7 Evaluation of response to treatment of a non-Hodgkin lymphoma in the tibia in a 27-year-old man. Before treatment: (a) Sagittal STIR MR image shows a large heterogeneous hyperintense intraosseous tumor extending into the soft tissues (*red arrows*). (b) Axial T1-weighted fat-suppressed (fs) image after Gd-DTPA injection shows solid enhancing mass extending to soft tissues (*blue arrows*). (c) Axial DWI shows hyperintense signal intensity mass (*yellow arrows*). (d) ADC map shows restricted diffusion of the tumor (*red arrows*) and $ADC=0.62 \times 10^{-3} \text{ mm}^2/\text{s}$. After

8 months' treatment: (e) Sagittal T1-weighted fat-suppressed image after Gd-DTPA injection shows heterogeneous enhancing intraosseous tumor without extension into the soft tissues (*red arrows*). (f) Axial T1-weighted fat-suppressed (fs) image after Gd-DTPA injection shows heterogeneous enhancing intraosseous lesion (*blue arrows*). (g) Axial DWI shows hyperintense signal intensity (T2 effect) (*yellow arrows*). (h) ADC map shows facilitated diffusion of the tumor (*red arrows*) and $ADC=2.2 \times 10^{-3} \text{ mm}^2/\text{s}$, suggesting tumor necrosis and good response to treatment

The use of conventional MR imaging on follow-up of treated musculoskeletal soft tissue masses is traditionally based on anatomic approaches and has significant limitations, since the mass may increase in size due to hemorrhage and edema, and both viable tumor and posttreatment scar tissue enhance after contrast agent administration [26].

Advanced MRI is capable of detecting early cellular changes in treated tumors that precede morphologic response, such as intracellular necrosis [3, 27, 28].

The advent of chemical shift MR imaging (inphase and opposed-phase imaging), diffusion-weighted imaging, perfusion imaging, and MR spectroscopy has forward the role of MR to characterize malignant lesions and assess them after treatment [25].

Cellular death and vascular changes in response to treatment precede the changes of the lesion size; thus, advanced imaging such as DWI and perfusion could provide earlier identification between patients with a poor treatment response from those with tumor recurrence [29]. Functional imaging

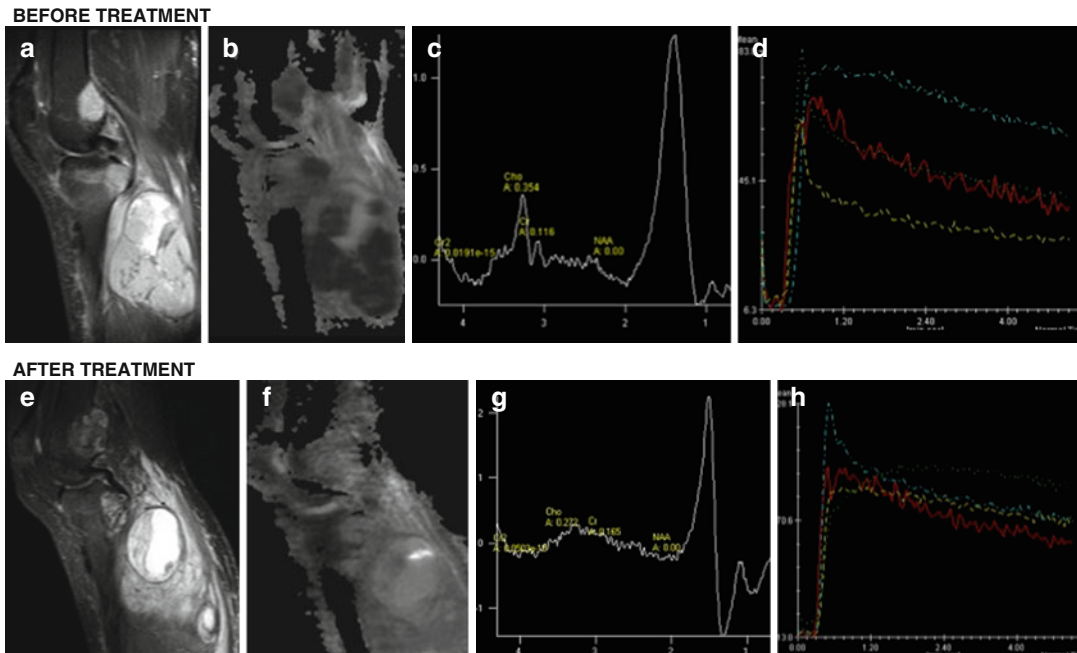


Fig. 55.8 Follow-up examination of a synovial sarcoma of the knee. Pretreatment images (a–d) and posttreatment images (e–h) are shown. Pretreatment images: (a) Sagittal fat suppressed proton density MR image shows a mass in the posterior soft tissue of the knee. (b) Sagittal ADC map image shows restricted diffusion ($ADC=0.86 \times 10^{-3} \text{ mm}^2/\text{s}^2$), suggesting malignant tumor. (c) MR spectroscopy shows high levels of choline. (d) TIC shows a type IV curve (dashed yellow, blue and green lines), indicating rapid enhancement. The type IV curve (red) represent the artery. Slope = 175 % for minute.

Posttreatment images: (e) sagittal fat suppressed proton density MR image shows a reduction of the tumor, of the restricted diffusion areas (f), and of the levels of choline in MR spectroscopy (g). (h) TIC shows a type IV curve (dashed blue line), still indicating rapid enhancement, suggesting viable cells with hypervascularity and consequently poor response to treatment. The type IV curve (red) represent the artery. Slope = 210 % for minute. Note that the tumor presented less than 40 % of reduction in slope value, also indicating poor response to treatment

might provide an opportunity to adjust individual treatment regimens more rapidly, sparing patients the unnecessary morbidity, expense, and delays in the initiation of effective treatment [30].

Previous reports described an effective anti-cancer therapy that resulted in tumor lysis, loss of membrane integrity, increased extracellular space, and increase in water molecule diffusion. All these changes resulted in an increase in ADC values [31, 32].

Preclinical and clinical studies have reported on the usefulness of DWI as a sensitive biomarker capable of detecting early cellular changes in treated tumors that precede morphologic response [27, 28]. In musculoskeletal tumors, successful therapy has been associated with increased ADC values [33–35].

The DWI technique is also being used to assess the activity of residual disease after treatment and to detect early recurrence at a time when a salvage therapy may still be effective [26].

Differentiation of post-therapeutic soft tissue changes and residual or recurrent tumor is a common diagnostic problem because these abnormalities have the same appearance in morphologic imaging (high signal intensity on T2-weighted and short tau inversion recovery images and a low signal intensity on T1-weighted SE images) [36].

Baur and colleagues [36] evaluated the signal characteristics of recurring solid soft tissue tumors and post-therapeutic soft tissue changes with DWI and demonstrated that post-therapeutic soft tissue changes showed a significantly higher diffusion than viable recurrent tumors. This is an expected

finding because solid tumors demonstrate high cellularity and intact cell membranes, whereas as antineoplastic therapy progresses successfully, the cellularity within the tumor decreases and cell membranes lose their integrity [37].

A static contrast-enhanced MR imaging does not predict the percentage of necrosis in a tumor after treatment because sarcomas show pathologic treatment response in the form of hyaline fibrosis, necrosis, and granulation tissue [38], and these alterations, as viable tumor, usually also enhance with intravenous contrast agent administration.

Dynamic contrast-enhanced MR imaging is the method of choice to monitor preoperative response to chemotherapy. Poor and good responders to chemotherapy can be detected on first-pass, subtraction images or the assessment of the time/intensity curves over time [10].

The purpose of MR examination is to detect local tumor recurrence or residual tumor tissue and to differentiate recurrence from reactive tissue. Tumor recurrence enhances fast during the first pass, whereas reactive tissue enhances later and more slowly [10]. In soft tissue sarcomas, focal areas of early and rapidly progressive enhancement correspond to residual viable or recurrent tumor. In contrast, dynamic studies showing no areas of early enhancement indicate a good response (Fig. 55.8) [10].

Radiation therapy can induce neovascularization, resulting increased perfusion in the irradiated area. Differentiation of a reactive mass with young granulation tissue from residual tumor tissue or tumor recurrence may be difficult in the first 3–6 months after irradiation of a sarcoma [10].

Follow-up examinations are necessary because perfusion of a reactive mass decreases, whereas residual tumor tissue grows and remains highly vascularized [10].

Conclusion

Advanced MR imaging is an important tool for diagnosing musculoskeletal tumors when used together with conventional MR imaging and the clinical history of the patient, avoiding unnecessary biopsies, facilitating early treatment, and improving patient outcome.

References

1. Costa FM, et al. Advanced magnetic resonance imaging techniques in the evaluation of musculoskeletal tumors. *Radiol Clin North Am.* 2011;49(6):1325–58, vii–viii.
2. Calleja M, et al. MRI of superficial soft tissue masses: analysis of features useful in distinguishing between benign and malignant lesions. *Skeletal Radiol.* 2012; 41(12):1517–24.
3. Costa FM, et al. Diffusion-weighted magnetic resonance imaging for the evaluation of musculoskeletal tumors. *Magn Reson Imaging Clin N Am.* 2011;19(1): 159–80.
4. Dinauer PA, et al. Pathologic and MR imaging features of benign fibrous soft-tissue tumors in adults. *Radiographics.* 2007;27(1):173–87.
5. Lee JC, et al. Aggressive fibromatosis: MRI features with pathologic correlation. *AJR Am J Roentgenol.* 2006;186(1):247–54.
6. Kransdorf MJ, Murphey MD. Imaging of soft tissue tumors. In: Mc Allister L, Barrett K, editors. *Imaging of soft tissue tumors.* Philadelphia: Lippincott Williams & Wilkins; 2006. p. 38–79.
7. Harish S, et al. MR imaging of skeletal soft tissue infection: utility of diffusion-weighted imaging in detecting abscess formation. *Skeletal Radiol.* 2011;40(3):285–94.
8. Oka K, et al. Ability of diffusion-weighted imaging for the differential diagnosis between chronic expanding hematomas and malignant soft tissue tumors. *J Magn Reson Imaging.* 2008;28(5): 1195–200.
9. Verstraete KL, et al. Benign and malignant musculoskeletal lesions: dynamic contrast-enhanced MR imaging—parametric “first-pass” images depict tissue vascularization and perfusion. *Radiology.* 1994; 192(3):835–43.
10. Verstraete KL, Lang P. Bone and soft tissue tumors: the role of contrast agents for MR imaging. *Eur J Radiol.* 2000;34(3):229–46.
11. Maeda M, et al. Soft-tissue tumors evaluated by line-scan diffusion-weighted imaging: influence of myxoid matrix on the apparent diffusion coefficient. *J Magn Reson Imaging.* 2007;25(6): 1199–204.
12. Nagata S, et al. Usefulness of diffusion-weighted MRI in differentiating benign from malignant musculoskeletal tumors. *Nippon Igaku Hoshasen Gakkai Zasshi.* 2005;65(1):30–6.
13. Nagata S, et al. Diffusion-weighted imaging of soft tissue tumors: usefulness of the apparent diffusion coefficient for differential diagnosis. *Radiat Med.* 2008;26(5):287–95.
14. van Rijswijk CS, et al. Diffusion-weighted MRI in the characterization of soft-tissue tumors. *J Magn Reson Imaging.* 2002;15(3):302–7.

15. Sundaram M, et al. Myxoid liposarcoma: magnetic resonance imaging appearances with clinical and histological correlation. *Skeletal Radiol.* 1990;19(5):359–62.
16. O’Keeffe F, et al. Radiological features of extraskelatal Ewing sarcoma. *Br J Radiol.* 1990;63(750):456–60.
17. Bracke P, et al. Soft tissue lymphoma. In: De Schepper AM, Vanhoenacker F, Gielen J, Parizel PM, editors. *Imaging of soft tissue tumors.* 3rd ed. Berlin: Springer; 2006. p. 462–9.
18. Laffan EE, et al. Pediatric soft-tissue tumors and pseudotumors: MR imaging features with pathologic correlation: part 2. Tumors of fibroblastic/myofibroblastic, so-called fibrohistiocytic, muscular, lymphomatous, neurogenic, hair matrix, and uncertain origin. *Radiographics.* 2009;29(4):e36.
19. Doganay S, et al. The role of MRS in the differentiation of benign and malignant soft tissue and bone tumors. *Eur J Radiol.* 2011;79(2):e33–7.
20. Wang CK, et al. Characterization of bone and soft-tissue tumors with in vivo 1H MR spectroscopy: initial results. *Radiology.* 2004;232(2):599–605.
21. Guo AC, et al. Lymphomas and high-grade astrocytomas: comparison of water diffusibility and histologic characteristics. *Radiology.* 2002;224(1):177–83.
22. Nakayama T, et al. Usefulness of the calculated apparent diffusion coefficient value in the differential diagnosis of retroperitoneal masses. *J Magn Reson Imaging.* 2004;20(4):735–42.
23. Toh CH, et al. Primary cerebral lymphoma and glioblastoma multiforme: differences in diffusion characteristics evaluated with diffusion tensor imaging. *AJNR Am J Neuroradiol.* 2008;29(3):471–5.
24. Fletcher BD, et al. Pediatric musculoskeletal tumors: use of dynamic, contrast-enhanced MR imaging to monitor response to chemotherapy. *Radiology.* 1992;184(1):243–8.
25. Fayad LM, et al. Musculoskeletal tumors: how to use anatomic, functional, and metabolic MR techniques. *Radiology.* 2012;265(2):340–56.
26. Padhani AR, Khan AA. Diffusion-weighted (DW) and dynamic contrast-enhanced (DCE) magnetic resonance imaging (MRI) for monitoring anticancer therapy. *Target Oncol.* 2010;5(1):39–52.
27. Roth Y, et al. High-b-value diffusion-weighted MR imaging for pretreatment prediction and early monitoring of tumor response to therapy in mice. *Radiology.* 2004;232(3):685–92.
28. Thoeny HC, et al. Diffusion-weighted MR imaging in monitoring the effect of a vascular targeting agent on rhabdomyosarcoma in rats. *Radiology.* 2005;234(3):756–64.
29. Padhani AR, et al. Diffusion-weighted magnetic resonance imaging as a cancer biomarker: consensus and recommendations. *Neoplasia.* 2009;11(2):102–25.
30. Kwee TC, et al. Cancer imaging: novel concepts in clinical magnetic resonance imaging. *J Intern Med.* 2010;268(2):120–32.
31. Koh DM, et al. Practical aspects of assessing tumors using clinical diffusion-weighted imaging in the body. *Magn Reson Med Sci.* 2007;6(4):211–24.
32. Moffat BA, et al. Diffusion imaging for evaluation of tumor therapies in preclinical animal models. *MAGMA.* 2004;17(3–6):249–59.
33. Dudeck O, et al. Diffusion-weighted magnetic resonance imaging allows monitoring of anticancer treatment effects in patients with soft-tissue sarcomas. *J Magn Reson Imaging.* 2008;27(5):1109–13.
34. Hayashida Y, et al. Monitoring therapeutic responses of primary bone tumors by diffusion-weighted image: initial results. *Eur Radiol.* 2006;16(12):2637–43.
35. Uhl M, et al. Osteosarcoma: preliminary results of in vivo assessment of tumor necrosis after chemotherapy with diffusion- and perfusion-weighted magnetic resonance imaging. *Invest Radiol.* 2006;41(8):618–23.
36. Baur A, et al. Diffusion-weighted imaging of tumor recurrences and posttherapeutic soft-tissue changes in humans. *Eur Radiol.* 2001;11(5):828–33.
37. Bley TA, et al. Diffusion-weighted MR imaging in musculoskeletal radiology: applications in trauma, tumors, and inflammation. *Magn Reson Imaging Clin N Am.* 2009;17(2):263–75.
38. Roberge D, et al. Radiological and pathological response following pre-operative radiotherapy for soft-tissue sarcoma. *Radiother Oncol.* 2010;97(3):404–7.